

# Decarboxylation and Tandem Reduction/Decarboxylation Pathways to Substituted Phenols from Aromatic Carboxylic Acids Using Bimetallic Nanoparticles on Supported Ionic Liquid Phases as Multifunctional Catalysts

Natalia Levin,<sup>§</sup> Lisa Goclik,<sup>§</sup> Henrik Walschus, Neha Antil, Alexis Bordet,\* and Walter Leitner\*



Cite This: *J. Am. Chem. Soc.* 2023, 145, 22845–22854



Read Online

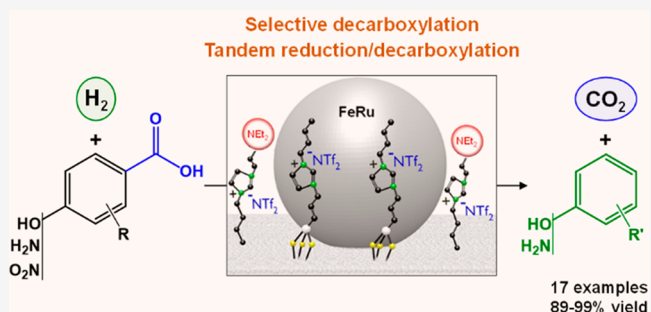
ACCESS |

Metrics & More

Article Recommendations

Supporting Information

**ABSTRACT:** Valuable substituted phenols are accessible via the selective decarboxylation of hydroxybenzoic acid derivatives using multifunctional catalysts composed of bimetallic iron–ruthenium nanoparticles immobilized on an amine-functionalized supported ionic liquid phase ( $\text{Fe}_{25}\text{Ru}_{75}@\text{SILP+IL-NEt}_2$ ). The individual components of the catalytic system are assembled using a molecular approach to bring metal and amine sites into close contact on the support material, providing high stability and high decarboxylation activity. Operating under a hydrogen atmosphere was found to be essential to achieve high selectivity and yields. As the catalyst materials enable also the selective hydrogenation and hydrodeoxygenation of various additional functional groups (i.e., formyl, acyl, and nitro substituents), direct access to the corresponding phenols can be achieved via integrated tandem reactions. The approach opens versatile synthetic pathways for the production of valuable phenols from a wide range of readily available substrates, including compounds derived from lignocellulosic biomass.



## INTRODUCTION

Phenol and its derivatives such as alkylphenols and aminophenols are important compounds that find widespread application in all areas of the chemical industry, including the production of commodities, fine chemicals, agrochemicals, and pharmaceuticals.<sup>1–9</sup> Nowadays, more than 99% of the world's phenol production (11 million tons in 2018) arises from the cumene process, where the petrochemical feedstocks benzene and propene are converted into phenol and acetone.<sup>3</sup> Alkylphenols are typically produced through the direct alkylation of phenol derivatives with olefins.<sup>3,10</sup> However, this pathway suffers from limited substrate scope.<sup>11–14</sup> Alternatively, the direct alkylation of phenol with alkyl halides requires harsh conditions and offers poor chemo- and regioselectivity.<sup>10</sup> The selective amination of phenol to produce aminophenols also remains a challenge.<sup>15–18</sup> Therefore, alternative methods to synthesize phenols have been actively researched. For example, the catalytic cleavage of lignin-derived diaryl ethers and lignin model compounds can lead to alkylphenols but current catalytic systems still suffer from low selectivity,<sup>19–22</sup> narrow substrate scope,<sup>22–24</sup> low catalyst stability,<sup>21</sup> or poor recyclability.<sup>24</sup> The selective reduction of vinylphenols has also been proposed but is hampered by the limited access and high costs of the starting materials.<sup>25,26</sup>

In this context, we envisaged to access phenol, alkylphenols, and aminophenols through the selective decarboxylation of hydroxybenzoic acid derivatives (HBAs), including substrates that can be obtained from the oxidative depolymerization of lignin or through biosynthesis<sup>27</sup> such as 4-hydroxybenzoic acid, vanillic acid, and syringic acid.<sup>28–30</sup> In addition, the tandem combination of the selective decarboxylation with hydrogenation/hydrodeoxygenation of easily accessible acyl, formyl, and nitro-functionalized HBAs<sup>31–33</sup> was explored in order to obtain alkylphenols and aminophenols. The required multifunctional catalytic system was designed on the basis of bimetallic FeRu nanoparticles supported on silica modified with amino-substituted ionic liquids ( $\text{Fe}_{25}\text{Ru}_{75}@\text{SILP+IL-NEt}_2$ ) (Figure 1).

## RESULTS AND DISCUSSION

**Catalyst Design.** Unlocking the potential of the proposed synthetic pathways requires multifunctional catalytic systems

Received: August 31, 2023

Published: October 10, 2023



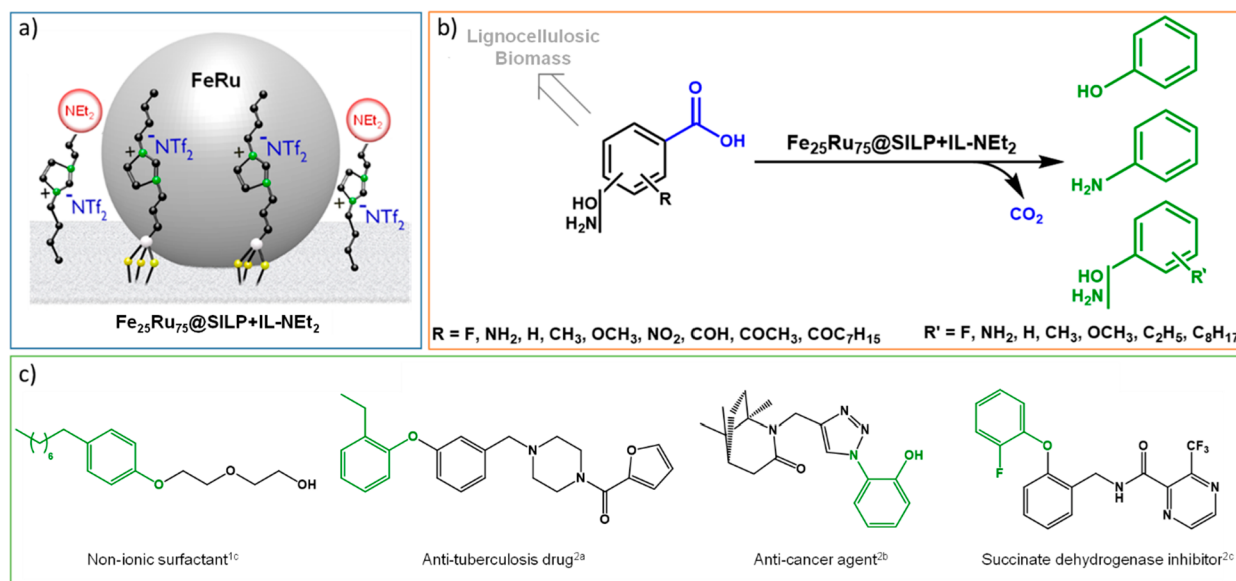


**Figure 1.** General approach in this study. (a) Illustration of the bimetallic bifunctional  $\text{Fe}_{25}\text{Ru}_{75}@\text{SILP+IL-NEt}_2$  catalyst, (b) proposed pathway for the synthesis of phenols through selective decarboxylation of hydroxybenzoic acid derivatives, and (c) examples of applications for phenol derivatives in pharmaceutical products.

capable of decarboxylating and hydrogenating and hydrode oxygenating substrates while leaving the aromatic ring untouched. Selective decarboxylation and reduction processes have already been investigated individually; however, to the best of our knowledge, there is no existing approach capable of combining them in a single catalytic system. The decarboxylation of aromatic acids is known to be an exergonic reaction favored entropically at low partial pressures of  $\text{CO}_2$ . The  $\Delta G$  of the reaction of decarboxylation of 4-hydroxybenzoic acid was estimated to be  $-17.7 \text{ kcal}\cdot\text{mol}^{-1}$  through density functional theory (DFT) calculations (see Table S1 in the Supporting Information for details). The model used was validated by comparing values estimated for benzoic acid and chlorobenzoic acid to published data (Table S1).<sup>34,35</sup> While decarboxylation of aromatic carboxylic acids is typically performed using transition-metal catalysts<sup>36–42</sup> based on metals such as Cu,<sup>37,38</sup> Ag,<sup>39</sup> Au,<sup>40</sup> Pd,<sup>41</sup> or Rh,<sup>42</sup> base-catalyzed decarboxylation reactions using amines were also reported for aromatic substrates bearing appropriate functional groups stabilizing the intermediate carbanion.<sup>43–45</sup> At present, however, examples of selective decarboxylation of HBAs are scarce in the literature, and limited to narrow substrate scopes and low yields.<sup>20,37,45–48</sup> For example, attempts to decarboxylate 4-HBA, vanillic acid, and syringic acid using Cu-based catalysts<sup>20</sup> or ILs<sup>47,48</sup> gave only yields up to 50%. On the other hand, metal nanoparticles immobilized on molecularly modified surfaces<sup>49</sup> have been shown to act as excellent catalysts for hydrogenation,<sup>50–57</sup> hydrode oxygenation<sup>58–62</sup> and hydrog enolysis reactions.<sup>19</sup> The combination of noble metals with excellent hydrogenation properties (e.g., Ru, Rh, etc.) with their more oxophilic 3d congeners (e.g., Fe, Co, etc.) was recently shown to produce bimetallic NPs with enhanced C=O hydrogenation activity, while suppressing aromatic ring hydrogenation.<sup>49,50,53,57</sup> In particular, the use of bimetallic FeRu-nanoparticles on ionic-liquid-modified silica support ( $\text{Fe}_{25}\text{Ru}_{75}@\text{SILP}$ ) catalyst was found capable of hydrode oxygenating acetophenone derivatives to alkylated aromatic products.<sup>59,60</sup> The flexibility of the NPs@SILP catalytic

platform for further customization prompted us to attempt the combination of FeRu NPs with the amine-functionalized SILP to integrate decarboxylation and hydrogenation capacity in a single material (Figure 1a).

**Catalyst Synthesis and Characterization.** The new multifunctional catalyst  $\text{Fe}_{25}\text{Ru}_{75}@\text{SILP+IL-NEt}_2$  was assembled in a versatile manner through the physisorption of the basic ionic liquid 1-[2-(diethylamino)ethyl]-3-butylimidazolium bis(trifluoromethane)sulfonamide (IL-NEt<sub>2</sub>) on the previously reported  $\text{Fe}_{25}\text{Ru}_{75}@\text{SILP}$  material.<sup>50</sup> In brief, the preparation of  $\text{Fe}_{25}\text{Ru}_{75}@\text{SILP}$  involved the condensation of [1-butyl-3-(3-triethoxy-silylpropyl)-imidazolium]NTf<sub>2</sub> with dehydroxylated SiO<sub>2</sub>. This molecular modifier is a typical imidazolium-based IL used in many precedent studies,<sup>50–53,58–60</sup> and the NTf<sub>2</sub> anion was selected for its stability, hydrophobicity, low nucleophilicity, non-coordinating, and redox innocent nature.<sup>63–66</sup> The synthetic procedure continues with the *in situ* reduction of a mesitylene solution of  $\{\text{Fe}[\text{N}(\text{Si}(\text{CH}_3)_3)_2]\}_2$  and  $[\text{Ru}(\text{cod})(\text{cot})]$  (cod = cyclooctadiene; cot = cyclooctatriene) under an atmosphere of H<sub>2</sub> (3 bar) at 150 °C (for the detailed procedure, see the Supporting Information). The oxidation state and alloy extent of the  $\text{Fe}_{25}\text{Ru}_{75}$  NPs in  $\text{Fe}_{25}\text{Ru}_{75}@\text{SILP}$  were previously studied by XANES and EXAFS, evidencing zerovalent Fe and Ru atoms organized in a homophilic bimetallic structure.<sup>50</sup> The newly synthesized amine functionalized IL-NEt<sub>2</sub> showed basic properties in water, with an experimentally determined pK<sub>aH</sub> value of  $7.21 \pm 0.01$  (expressed as the strength of its conjugated acid) (Figure S1), consistent with DFT calculations (7.3, Table S2). Its physisorption to prepare the bifunctional catalyst ( $\text{Fe}_{25}\text{Ru}_{75}@\text{SILP+IL-NEt}_2$ ) was achieved by stirring a suspension of  $\text{Fe}_{25}\text{Ru}_{75}@\text{SILP}$  and IL-NEt<sub>2</sub> in acetone at room temperature, followed by removal of the solvent under a vacuum.<sup>58</sup> After varying the loading of physisorbed IL-NEt<sub>2</sub> (Table S3), it was fixed to  $0.731 \pm 0.001 \text{ mmol}\cdot\text{g}^{-1}$  for the rest of the study, corresponding to an IL-NEt<sub>2</sub>/metal molar ratio of 2.9.

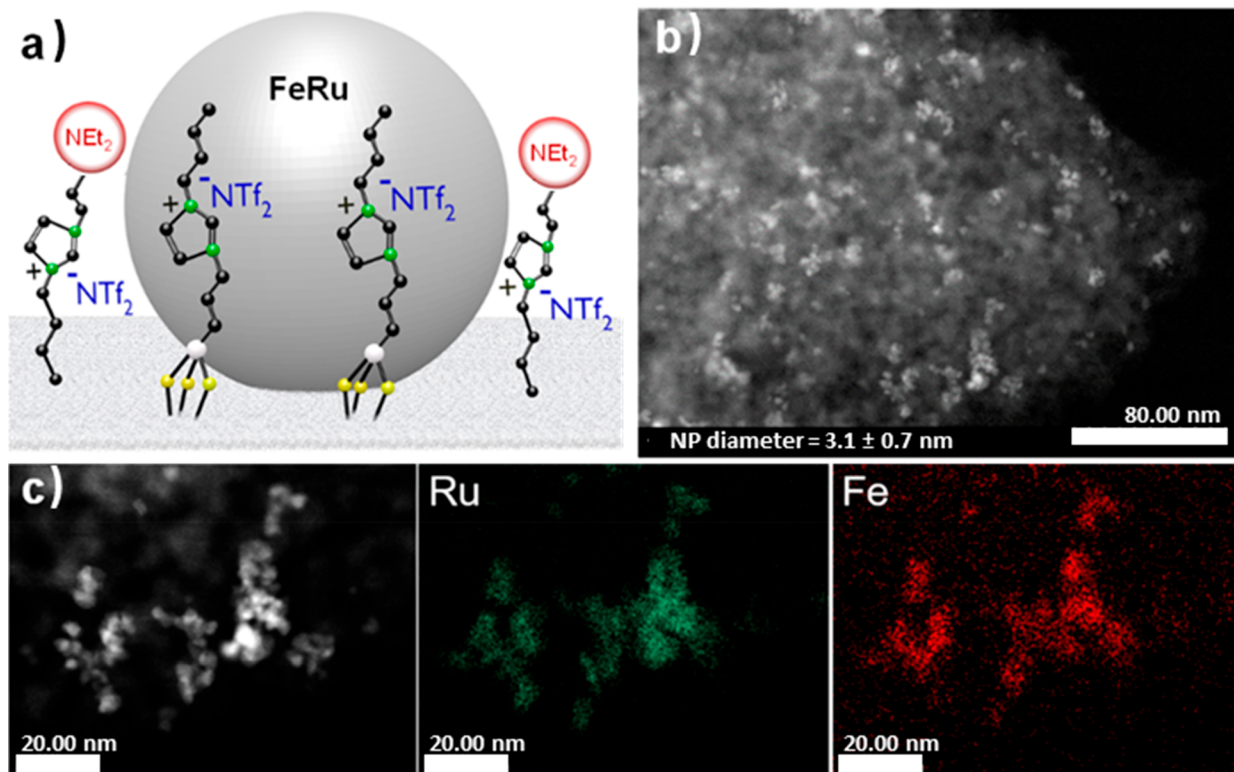


**Figure 2.**  $\text{Fe}_{25}\text{Ru}_{75}$ @SILP+IL-NEt<sub>2</sub> bimetallic bifunctional catalytic system. (a) Illustration, (b) STEM-HAADF image, (c) STEM-HAADF-EDS elemental mapping (green = Ru, red = Fe).

As expected, the BET surface area ( $36 \text{ m}^2 \cdot \text{g}^{-1}$ ) and the pore volume ( $0.13 \text{ m}^3 \cdot \text{g}^{-1}$ ) measured by N<sub>2</sub> adsorption experiments were significantly reduced upon the physisorption of IL-NEt<sub>2</sub> on  $\text{Fe}_{25}\text{Ru}_{75}$ @SILP (Table S4). Titration of the amount of accessible amine functionalities on  $\text{Fe}_{25}\text{Ru}_{75}$ @SILP+IL-NEt<sub>2</sub> gave  $0.49 \pm 0.01 \text{ mmol} \cdot \text{g}^{-1}$ , which corresponds to  $66.4 \pm 0.1\%$  of the theoretical total amount for quantitative adsorption. Characterization of  $\text{Fe}_{25}\text{Ru}_{75}$ @SILP+IL-NEt<sub>2</sub> by scanning transmission electron microscopy in high angle annular dark field (STEM-HAADF) associated with energy dispersive X-ray spectroscopy (EDS) showed the presence of small (3.1 nm) bimetallic NPs containing Fe and Ru (Figure 2).

Scanning electron microscopy (SEM) with EDS confirmed the expected metal ratio and metal loading ( $0.34 \pm 0.03 \text{ mmol} \cdot \text{g}^{-1}$ , Table S4). Thus, physisorption did not affect significantly the metal loading or ratio, nor the size of the metal NPs, even though they were slightly more aggregated than on the pristine  $\text{Fe}_{25}\text{Ru}_{75}$ @SILP material.<sup>50</sup>

**Catalytic Study. Identification of Reaction Parameters.** The catalytic performances of the bifunctional  $\text{Fe}_{25}\text{Ru}_{75}$ @SILP+IL-NEt<sub>2</sub> catalyst as well as several reference materials were first investigated for the decarboxylation of 4-hydroxybenzoic acid (**1**) as a model reaction (Table 1). The standard conditions were set to 175 °C, 18 h, heptane as solvent, and 65 equiv of substrate with respect to the total metal loading (30 equiv relative to the amine groups of IL-NEt<sub>2</sub>). Performing this reaction without applying any pressure resulted in an extremely low mass balance (Table 1, entry 1). Using 50 bar of inert gas pressure (N<sub>2</sub> or Ar) allowed observing significant conversion of **1** to phenol (**1a**) yet still with low yields (18% and 10%, respectively) and unclosed mass balances (Table 1, entries 2 and 3). In contrast, **1** was fully and selectively decarboxylated using  $\text{Fe}_{25}\text{Ru}_{75}$ @SILP+IL-NEt<sub>2</sub> under a H<sub>2</sub>

**Table 1. Decarboxylation of **1** Using  $\text{Fe}_{25}\text{Ru}_{75}$ @SILP+IL-NEt<sub>2</sub> and Various Reference Materials<sup>a</sup>**

#	Catalyst	Applied gas	X [%]	Y <sub>1a</sub> [%]
1	$\text{Fe}_{25}\text{Ru}_{75}$ @SILP+IL-NEt <sub>2</sub>	None	-	-
2	$\text{Fe}_{25}\text{Ru}_{75}$ @SILP+IL-NEt <sub>2</sub>	N <sub>2</sub>	$18 \pm 5$	$18 \pm 5$
3	$\text{Fe}_{25}\text{Ru}_{75}$ @SILP+IL-NEt <sub>2</sub>	Ar	10	10
4	$\text{Fe}_{25}\text{Ru}_{75}$ @SILP+IL-NEt <sub>2</sub>	H <sub>2</sub>	>99	>99
5	None	H <sub>2</sub>	0	0
6	$\text{Fe}_{25}\text{Ru}_{75}$ @SILP	H <sub>2</sub>	$4 \pm 1$	$4 \pm 1$
7	SILP+IL-NEt <sub>2</sub>	H <sub>2</sub>	$58 \pm 2$	$58 \pm 2$
8	$\text{Fe}_{40}\text{Ru}_{60}$ @SILP+IL-NEt <sub>2</sub>	H <sub>2</sub>	$33 \pm 2$	$33 \pm 2$
9	$\text{Fe}_{60}\text{Ru}_{40}$ @SILP+IL-NEt <sub>2</sub>	H <sub>2</sub>	$37 \pm 1$	$37 \pm 1$
10	$\text{Fe}_{100}$ @SILP	H <sub>2</sub>	0	0
11	$\text{Ru}_{100}$ @SILP	H <sub>2</sub>	>99	0 <sup>b</sup>
12	$\text{Fe}_{25}\text{Ru}_{75}$ @SiO <sub>2</sub>	H <sub>2</sub>	>99	39 <sup>c</sup>
13	$\text{Fe}_{25}\text{Ru}_{75}$ @SILP+IL-NEt <sub>2</sub> <sup>d</sup>	H <sub>2</sub>	>99	>99
14	$\text{Fe}_{25}\text{Ru}_{75}$ @SILP+IL-SO <sub>3</sub> H	H <sub>2</sub>	0	0
15	$\text{Fe}_{25}\text{Ru}_{75}$ @SILP+IL-NH <sub>2</sub>	H <sub>2</sub>	6	6
16	$\text{Fe}_{25}\text{Ru}_{75}$ @SILP + SILP+IL-NEt <sub>2</sub>	H <sub>2</sub>	$68 \pm 3$	$68 \pm 3$
17	$\text{Fe}_{25}\text{Ru}_{75}$ @SILP+IL-NEt <sub>2</sub> <sup>e</sup>	D <sub>2</sub> <sup>e</sup>	>99	>99

<sup>a</sup>Standard reaction conditions: Catalyst (metal content: 0.0034 mmol), substrate (0.221 mmol, 65 equiv compared to metal), solvent = heptane (0.5 mL), 175 °C, H<sub>2</sub> (50 bar), 18 h, 500 rpm; X = conversion, Y = yield, determined by GC-FID using tetradecane as internal standard. Variations are shown for two independent experiments. <sup>b</sup>Product = cyclohexanol (99%). <sup>c</sup>Byproducts = cyclohexanol (38%) and cyclohexane (23%). <sup>d</sup>With Br anion. <sup>e</sup>20 bar of D<sub>2</sub>, 200 °C.

atmosphere (50 bar), affording **1a** in quantitative yield without reduction of the aromatic moiety (**Table 1**, entry 4).

Without a catalyst, no conversion was observed under these conditions (**Table 1**, entry 5). Similarly, using the bimetallic  $\text{Fe}_{25}\text{Ru}_{75}@\text{SILP}$  catalyst without a physisorbed IL resulted in very low decarboxylation activity (4% yield, **Table 1**, entry 6). With SILP+IL-N<sub>Et</sub><sub>2</sub> in the absence of  $\text{Fe}_{25}\text{Ru}_{75}$  NPs, the conversion and yield of **1a** reached only 58% (**Table 1**, entry 7). Lowering the amount of Ru in the bimetallic particles in  $\text{Fe}_{40}\text{Ru}_{60}@\text{SILP+IL-N}(\text{Et})_2$  and  $\text{Fe}_{60}\text{Ru}_{40}@\text{SILP+IL-N}(\text{Et})_2$  resulted in lower conversions and yields (**Table 1**, entries 8 and 9). As expected,  $\text{Fe}_{100}@\text{SILP}$  gave no activity at all (**Table 1**, entry 10), while  $\text{Ru}_{100}@\text{SILP}$  led to complete hydrogenation of the aromatic ring (**Table 1**, entry 11). Bimetallic FeRu NPs prepared directly on silica ( $\text{Fe}_{25}\text{Ru}_{75}@\text{SiO}_2$ ) gave very low selectivity toward the formation of **1a** (**Table 1**, entry 12) accompanied by significant aromatic ring hydrogenation, indicating the presence of monometallic Ru-particles. This corroborates with the previously reported beneficial role of IL-modifiers to avoid segregated particles upon synthesis of bimetallic NPs.<sup>53,57</sup> Replacing the  $\text{NTf}_2$  anion by Br did not change the product distribution under these conditions (**Table 1**, entry 13). The recently reported acid-functionalized  $\text{Fe}_{25}\text{Ru}_{75}@\text{SILP+IL-SO}_3\text{H}$  catalyst<sup>58</sup> led to no reaction, evidencing the need for a base (**Table 1**, entry 14). Replacing the tertiary amine functionality of IL-N<sub>Et</sub><sub>2</sub> by a primary amine (IL-NH<sub>2</sub>, calculated  $\text{pK}_{\text{aH}}$  in water = 4.8, **Table S2**) led to a loss of catalytic activity (**Table 1**, entry 15). A physical mixture of  $\text{Fe}_{25}\text{Ru}_{75}@\text{SILP}$  and triethylamine ( $\text{pK}_{\text{aH}}$  in water = 10.7) afforded full conversion, while losing the potential for reusability (**Table S5**). Interestingly, using secondary and primary amines of similarly high basicity (i.e., diethylamine and butylamine  $\text{pK}_{\text{aH}}$  in water = 11.0 and 10.6, respectively) was also successful (**Table S5**). In contrast, lower activity was observed in the presence of a weaker base such as *N,N*-dimethylaniline (61% conversion,  $\text{pK}_{\text{aH}}$  in water = 5.1), and diphenylamine ( $\text{pK}_{\text{aH}}$  in water = 0.8) was found to be inactive (**Table S5**). These results indicate that the decarboxylation reaction can proceed smoothly in the presence of primary, secondary, or tertiary amine functionalities, as long as their basicity is sufficient.

Notably, a physical mixture of  $\text{Fe}_{25}\text{Ru}_{75}@\text{SILP}$  and metal-free SILP+IL-N<sub>Et</sub><sub>2</sub> also did not reach the level of performance of  $\text{Fe}_{25}\text{Ru}_{75}@\text{SILP+IL-N}(\text{Et})_2$  (68% conversion and yield, **Table 1**, entry 16), demonstrating the synergistic action induced by the intimate contact of the two functionalities.

In order to get additional insight into the beneficial role of the hydrogen atmosphere in the decarboxylation reaction, the reaction was performed under standard conditions in the presence of D<sub>2</sub> (20 bar).

Full conversion to phenol was observed in this case as well (**Table 1**, entry 17), and <sup>1</sup>H and <sup>13</sup>C NMR of the isolated product revealed deuterium incorporation in the *ortho* and *para* positions of the hydroxyl functionality (**Table S6** and **Figure S2**), with 78% of the product being deuterated in *para*. Exposing product **1a** to D<sub>2</sub> under standard reaction conditions led to H/D exchange in the *ortho* position to the hydroxyl functionality only (**Table S6** and **Figure S2**). This demonstrates that the deuterium incorporation in the *para* position occurs as a result of the decarboxylation process at this position. While no significant H/D exchange of the proton at the carboxylic acid functionality was observed within the first 1 h when 22% conversion was achieved, incorporation of D in

the product in the *para* position was already very significant (40% of the product, **Figure S3**). Analysis of the gas phase confirmed the release of CO<sub>2</sub> (**Figure S4**). These results indicate that the incorporation of D in the *para* position occurs from the gas phase during the decarboxylation reaction, potentially as a consequence of heterolytic activation of D<sub>2</sub> by the NPs generating D<sup>+</sup> assisted by the base.

To gain additional insight into the mechanism, time profiles of the decarboxylation of **1** were recorded using  $\text{Fe}_{25}\text{Ru}_{75}@\text{SILP+IL-N}(\text{Et})_2$  under H<sub>2</sub> and D<sub>2</sub> (**Figure 3**). The initial rate of

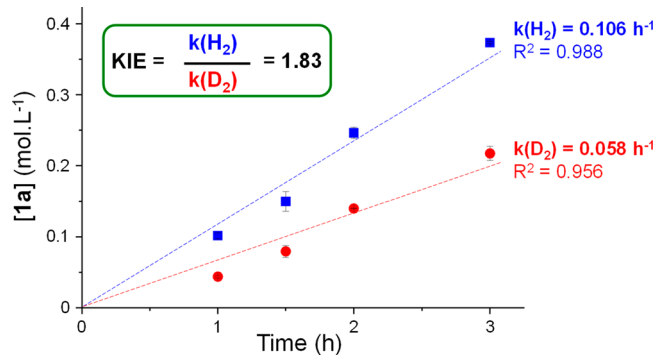


**Figure 3.** Determination of the kinetic isotope effect for the decarboxylation of **1** using  $\text{Fe}_{25}\text{Ru}_{75}@\text{SILP+IL-N}(\text{Et})_2$ . Reaction conditions: Catalyst (10 mg, metal content: 0.0034 mmol), **1** (0.221 mmol, 65 equiv compared to metal), heptane (0.5 mL), 175 °C, H<sub>2</sub> or D<sub>2</sub> (20 bar), 500 rpm; yield determined by GC-FID using tetradecane as internal standard. The selectivity is >99% in all cases, so conversion = yield. Data points represent average values, and error bars correspond to standard deviations.

the reaction was found to be noticeably higher under H<sub>2</sub> than under D<sub>2</sub>, resulting in an apparent normal kinetic isotope effect (KIE) of 1.83. This value is sensibly larger than the theoretical maximum for a secondary KIE (1.4),<sup>67</sup> pointing toward a primary KIE, and thus toward a rate-determining step dependent on the formation or the cleavage of a bond involving a hydrogen atom coming from the gas phase. Since the activation of gaseous hydrogen is mediated by  $\text{Fe}_{25}\text{Ru}_{75}$  NPs, this result is another strong indication of their crucial involvement in the decarboxylation process and supports the existence of a strong synergistic interaction between  $\text{Fe}_{25}\text{Ru}_{75}$  NPs and amine functionalities brought in intimate contact.

Interestingly, Lercher and co-workers recently showed that the decarboxylation activity of Pd/C could be enhanced by H<sub>2</sub> pretreatment.<sup>68</sup> Their method was focused on aryl-substituted aliphatic carboxylic acids having an  $\alpha$ -C–H group, and use of H<sub>2</sub> during the reaction resulted in undesired aromatic ring hydrogenation.

**Selective Decarboxylation of Aromatic Carboxylic Acids.** Based on these promising results, the  $\text{Fe}_{25}\text{Ru}_{75}@\text{SILP+IL-N}(\text{Et})_2$  catalyst was applied to a scope of benzoic acids possessing hydroxyl, methoxy, and amine substituents (**Table 2**).

Lignin-derived 4-hydroxybenzoic acid derivatives **1–3** were readily decarboxylated, giving the corresponding phenols (**1a–3a**) in excellent selectivity and yields (**Table 2**, entries 1–3). Substrates **4–6** with electron donating or withdrawing groups in position 3 were also quantitatively converted to the corresponding phenols (**Table 2**, entries 4–6). Similar results were obtained with salicylic acid (**7**), in which the hydroxyl functionality is in the *ortho* position. In sharp contrast, no conversion was observed when using 3-hydroxybenzoic acid

**Table 2.** Decarboxylation of Aromatic Carboxylic Acids<sup>a</sup>

$\text{R}^1\text{-C}_6\text{H}_3(\text{R}^2)\text{COOH} \xrightarrow[\text{T } ^\circ\text{C}, 50 \text{ bar H}_2, 18 \text{ h, heptane}]{\text{Fe}_{25}\text{Ru}_{75}@\text{SILP+IL-NEt}_2} \text{R}^1\text{-C}_6\text{H}_3(\text{R}^2)\text{R}^3$   
 $\text{R}^1: \text{H, OMe, Me, F, NH}_2, \text{OH} / \text{R}^2: \text{H, OH} / \text{R}^3: \text{H, OH, NH}_2$

#	Substrate	Product	T [°C]	X [%]	Y [%]
1			175	>99	>99 (91)
2			200	>99	>99
3			200	>99	>99 (95)
4			175	>99	>99
5			175	>99	>99
6			175	>99	>99
7			200	>99	>99
8			200	0	0
9			150	>99	>99

<sup>a</sup>Reaction conditions: Catalyst (10 mg, metal content: 0.0034 mmol), substrate (0.221 mmol, 65 equiv related to total metal loading), solvent = heptane (0.5 mL), H<sub>2</sub> (50 bar), 18 h, 500 rpm; Y = yield, X = conversion, determined by GD-FID using tetradecane as internal standard. Isolated yields in parentheses.

(8) as the substrate, suggesting that mesomeric effects are important to observe decarboxylation activity with Fe<sub>25</sub>Ru<sub>75</sub>@SILP+IL-NEt<sub>2</sub>. In the quest for sustainable synthetic pathways for the production of not only phenols but also aniline, the decarboxylation of anthranilic acid is an equally attractive and challenging pathway.<sup>69</sup> Notably, our catalytic system also showed excellent activity and selectivity for the decarboxylation of anthranilic acid (9) to give aniline in quantitative yield (Table 2, entry 9), showing that the decarboxylation activity of Fe<sub>25</sub>Ru<sub>75</sub>@SILP+IL-NEt<sub>2</sub> is not limited to hydroxybenzoic acid derivatives. In this case, the temperature was reduced to 150 °C to avoid side reactions (e.g., deamination). Straightforward isolation of analytically pure material from the reaction mixtures was demonstrated for products 1a and 3a (91 and 95% isolated yield, respectively). Notably, 2,6-dimethoxyphenol (3a) is used for the synthesis of cellular antiproliferate active agents and becomes thus accessible from lignin-derived syringic acid.<sup>70</sup>

**Tandem Reduction and Decarboxylation of Substituted Aromatic Carboxylic Acids.** Next, the potential of the Fe<sub>25</sub>Ru<sub>75</sub>@SILP+IL-NEt<sub>2</sub> catalyst for tandem reduction/decarboxylation of hydroxy and aminobenzoic acid derivatives possessing additional reducible functional groups was envisaged to exploit the capacity of hydrogen activation and

transfer at the FeRu NPs.<sup>50,59,60</sup> Under standard conditions, 3-acetyl-4-hydroxybenzoic (10) was selectively decarboxylated and hydrodeoxygenated directly to produce 2-ethylphenol (10a) in >99% yield (Table 3, entry 1). Following the reduction/decarboxylation for the nitro-substituted HBA 12 as a function of time clearly showed the sequential tandem reaction via 3-amino-4-hydroxybenzoic acid (6) as an intermediate (Figure 4). The reaction occurs smoothly to produce selectively 2-aminophenol (6a) in nearly quantitative yield (>99%) after 24 h. Adaptation of the standard reaction conditions (temperature, substrate equivalent, solvent) to ensure good solubility and to limit side-reactions allowed efficient conversion of a range of 2- and 4-hydroxybenzoic acid derivatives possessing acetyl, octanoyl, formyl, or nitro substituents (substrates 11–16, Table 3, entries 2–7). The corresponding phenol derivatives (11a–16a) were produced in excellent selectivity and yields (95–99%) and isolated for selected examples.

Also, in this case, replacing the hydroxyl by an amine functionality in 2-amino-5-acetylbenzoic acid (17) did not influence negatively the catalyst performance, and 4-ethylaniline (17a) was obtained in 89% yield (Table 3, entry 8). Interestingly, many of the products formed are valuable chemicals with widespread applications. In particular, 10a, 6a,

**Table 3.** Decarboxylation and Selective Reduction of Aromatic Carboxylic Acids<sup>a</sup>

The reaction scheme illustrates the conversion of aromatic carboxylic acids to their corresponding phenols or reduced products. The starting materials are substituted benzene rings with a carboxylic acid group (-COOH) at the para position. These are converted to either phenols (R' = H) or reduced products (R' = OH, NH<sub>2</sub>) depending on the reaction conditions. The catalyst used is  $\text{Fe}_{25}\text{Ru}_{75}@\text{SILP+IL-NEt}_2$ , which is applied at  $T^\circ\text{C}$ , 50 bar  $\text{H}_2$ , and 18 h in a specific solvent.

#	Substrate	Product	Solvent	Sub:Met	Sub:Am	T [°C]	X [%]	Y [%]
1	10	10a	heptane	65	30	175	>99 (89)	>99
2	11	4a	heptane	33	15	200	>99	>99
3	12	6a	heptane	65	30	150	>99 (77)	>99
4	13	13a	heptane	33	15	175	>99 (83)	>99
5	14	14a	decalin	33	15	200	>99 (85)	>99
6	15	15a	dioxane	33	15	200	>99	>99
7	16	16a	dioxane	33	15	200	>99	95 <sup>b</sup>
8	17	17a	mesitylene	33	15	200	>99	89 <sup>c</sup>

<sup>a</sup>Reaction conditions: Catalyst (10 mg, metal content: 0.0034 mmol), solvent = heptane (0.5 mL),  $\text{H}_2$  (50 bar), 18 h, 500 rpm. <sup>b</sup>11% aniline.

<sup>c</sup>Byproducts: dimers; Y = yield, X = conversion, determined by GC-FID using tetradecane as internal standard. Isolated yields in parentheses. Sub:Met = substrate to metal ratio, Sub:Am = substrate to amine ratio.

and 17a are building blocks used in the pharmaceutical industry for the synthesis of anti-tuberculosis drugs,<sup>7</sup> anticancer agents,<sup>8</sup> and fungicides,<sup>8</sup> respectively (Figure 1c). 14a is widely used in the production of nonionic surfactants (Figure 1c).<sup>3</sup> Using metal-free SILP+IL-NEt<sub>2</sub> as a catalyst for the conversion of 2-hydroxy-5-octanoylbenzoic acid (14) led only to decarboxylation, with 4'-hydroxyoctanophenone as a product (Table S7). This demonstrates the necessity to have  $\text{Fe}_{25}\text{Ru}_{75}$  NPs to perform tandem decarboxylation and hydrogenation/hydrodeoxygenation reactions.

**Catalyst Recycling and Stability.** Since leaching of physisorbed ionic liquids is a well-known issue in solution phase catalysis, the stability of  $\text{Fe}_{25}\text{Ru}_{75}@\text{SILP+IL-NEt}_2$  was carefully studied through recycling experiments using 4-hydroxybenzoic acid (1) as a model substrate (Figure 5). Between each cycle, a sample of the reaction mixture was taken, and the catalyst was washed with mesitylene. The reaction time was set to 6 h to ensure an incomplete conversion of the substrate and allow observing any change in

activity or selectivity upon recycling. The yield associated with the formation of phenol was fairly constant (48% on average) for at least five cycles without any makeup or regeneration. The fluctuations observed are presumably due to the recycling procedure adopted, during which traces of products may have stayed on the catalyst between each cycle (see the Supporting Information for the detailed recycling procedure). Characterization of the catalyst with quantitative SEM-EDS after five cycles did not evidence significant variations in the total metal loading or in the Fe:Ru ratio, indicating the absence of leaching of the metals (Table S8). TEM analysis showed no noticeable growth nor aggregation of the NPs. In future studies, potential changes in the NPs' bimetallic structure and electronic properties will be investigated by *ex situ* and operando X-ray absorption spectroscopy and magnetic measurements. N<sub>2</sub> adsorption experiments indicated that the textural properties (BET surface area, pore size, and pore volume) of  $\text{Fe}_{25}\text{Ru}_{75}@\text{SILP+IL-NEt}_2$  were conserved. Titration of the available amine functionalities evidenced a similar

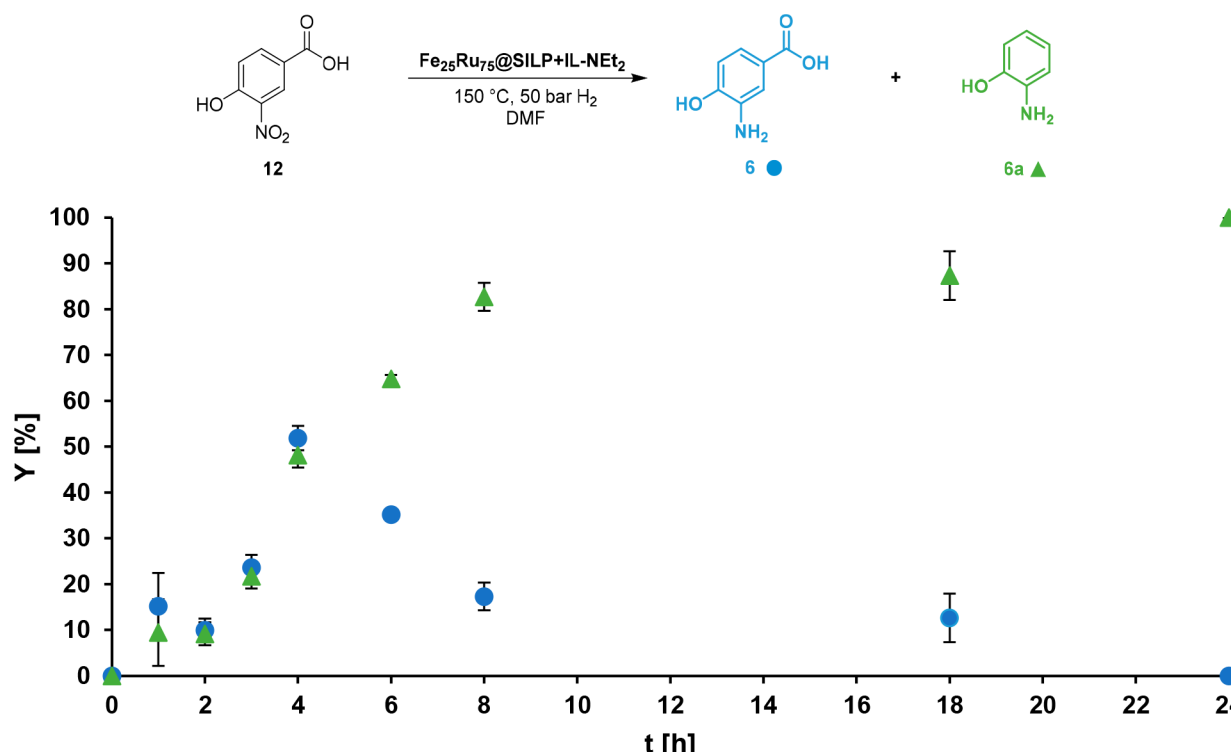


**Figure 4.** Time profile of the reduction and decarboxylation of 3-nitro-4-hydroxybenzoic acid (**12**) using  $\text{Fe}_{25}\text{Ru}_{75}@\text{SILP+IL-NEt}_2$ . Conditions: Catalyst (10 mg), substrate = 24.2 mg (30 equiv related to amine, 65 equiv related to total metal loading), 0.5 mL of DMF, 50 bar of  $\text{H}_2$ , 150 °C, 500 rpm. Y = Yield, determined by GD-FID using tetradecane as internal standard. Error bars represent the standard deviation for two experiments.

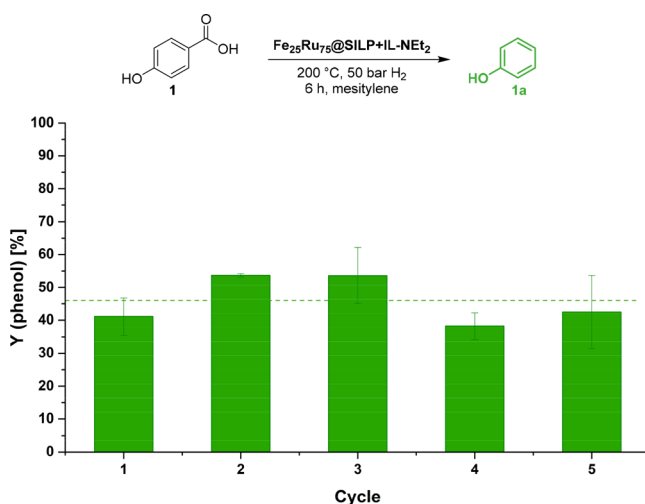


**Figure 5.** Catalyst recycling, decarboxylation of 4-hydroxybenzoic acid (**1**). Conditions:  $\text{Fe}_{25}\text{Ru}_{75}@\text{SILP+IL-NEt}_2$  (20 mg), substrate = 30.6 mg (30 equiv related to metal), 1 mL of mesitylene, 50 bar of  $\text{H}_2$ , 200 °C, 6 h, 500 rpm. Product yields were determined by GD-FID using tetradecane as internal standard. Selectivity toward **1a** >99%. Error bars represent the standard deviation for three experiments.

loading as that on the fresh catalyst, confirming the absence of leaching of the IL- $\text{NEt}_2$  under reaction conditions (Table S8). The analytical data indicate no sign of amidation of the carboxylic acid.

## CONCLUSION

In conclusion, the catalytic decarboxylation and tandem reduction/decarboxylation of hydroxy- and aminobenzoic acid derivatives were established as a versatile synthetic

pathway for the synthesis of substituted phenols and anilines. A molecular approach was used to assemble bimetallic FeRu NPs and basic amine functionalities on a single support to produce a multifunctional  $\text{Fe}_{25}\text{Ru}_{75}@\text{SILP+IL-NEt}_2$  catalytic system. Operating under a  $\text{H}_2$  atmosphere was found to be essential for high catalytic activity, and labeling experiments showed that protons from the gas phase are incorporated in the products during decarboxylation. This highlights the synergistic action of the amine functionalities and FeRu NPs, the first being responsible for the activation of the carboxylic acid functionality, while the second presumably assists the protonolysis for product release through  $\text{H}_2$  activation. Consequently, the hydrogen activation and proton transfer were exploited by integrating the decarboxylation with selective hydrogenation and hydrodeoxygenation of substituted substrates. The novel tandem reaction sequence expands significantly the scope of hydroxybenzoic acids that can be converted and thus the variety of accessible phenolic structures. This approach provides a promising alternative strategy for the synthesis of valuable phenol derivatives from readily available hydroxybenzoic acids including substrates that can be derived from biomass feedstock or through biosynthesis.

## ASSOCIATED CONTENT

### Supporting Information

The Supporting Information is available free of charge at <https://pubs.acs.org/doi/10.1021/jacs.3c09290>.

Supplementary Tables and Figures, and Experimental Section describing catalysts synthesis, characterization methods, and protocols for catalytic experiments (PDF)

## AUTHOR INFORMATION

### Corresponding Authors

**Alexis Bordet** – Max Planck Institute for Chemical Energy Conversion, 45470 Mülheim an der Ruhr, Germany;  [orcid.org/0000-0003-0133-3416](https://orcid.org/0000-0003-0133-3416); Email: [alexis.bordet@cec.mpg.de](mailto:alexis.bordet@cec.mpg.de)

**Walter Leitner** – Max Planck Institute for Chemical Energy Conversion, 45470 Mülheim an der Ruhr, Germany; Institut für Technische und Makromolekulare Chemie, RWTH Aachen University, 52074 Aachen, Germany;  [orcid.org/0000-0001-6100-9656](https://orcid.org/0000-0001-6100-9656); Email: [walter.leitner@cec.mpg.de](mailto:walter.leitner@cec.mpg.de)

### Authors

**Natalia Levin** – Max Planck Institute for Chemical Energy Conversion, 45470 Mülheim an der Ruhr, Germany;  [orcid.org/0000-0001-9567-8604](https://orcid.org/0000-0001-9567-8604)

**Lisa Goclik** – Max Planck Institute for Chemical Energy Conversion, 45470 Mülheim an der Ruhr, Germany; Institut für Technische und Makromolekulare Chemie, RWTH Aachen University, 52074 Aachen, Germany

**Henrik Walschus** – Max Planck Institute for Chemical Energy Conversion, 45470 Mülheim an der Ruhr, Germany

**Neha Antil** – Max Planck Institute for Chemical Energy Conversion, 45470 Mülheim an der Ruhr, Germany

Complete contact information is available at:

<https://pubs.acs.org/10.1021/jacs.3c09290>

### Author Contributions

<sup>§</sup>N.L., L.G.: These authors contributed equally.

### Funding

Open access funded by Max Planck Society.

### Notes

The authors declare no competing financial interest.

## ACKNOWLEDGMENTS

The authors acknowledge financial support by the Max Planck Society and by the Deutsche Forschungsgemeinschaft (DFG, German Research Foundation) under Germany's Excellence Strategy – Exzellenzcluster 2186 “The Fuel Science Center” ID:390919832. Furthermore, the authors thank Alina Jakubowski, Annika Gurowski, Justus Werkmeister, and Norbert Pfänder (MPI-CEC, Mülheim/Ruhr) for their support with the analytics and Dr. Christophe Fares for his help with the NMR measurements.

## REFERENCES

- (1) Hutchins, R. O.; Hutchins, M. K.; Fleming, I. *Comprehensive Organic Synthesis*; Elsevier: 1991.
- (2) Lorenc, F.; Lambeth, G.; Scheffer, W. *Alkylphenols*; John Wiley & Sons, Inc.: 2003.
- (3) Fiege, H.; Voges, H.-W.; Hamamoto, T.; Umemura, S.; Iwata, T.; Miki, H.; Fujita, Y.; Buysch, H.-J.; Garbe, D.; Paulus, W. Phenol Derivatives. *Ullmann's Encyclopedia of Industrial Chemistry* 2012, 503–519.
- (4) Liu, Y.; Baráth, E.; Shi, H.; Hu, J.; Camaioni, D. M.; Lercher, J. A. Solvent-Determined Mechanistic Pathways in Zeolite-H-BEA-Catalysed Phenol Alkylation. *Nat. Catal.* 2018, 1, 141–147.
- (5) Albuquerque, B. R.; Heleno, S. A.; Oliveira, M. B. P. P.; Barros, L.; Ferreira, I. C. F. R. Phenolic compounds: Current Industrial Applications, Limitations and Future Challenges. *Food Funct.* 2021, 12, 14–29.
- (6) Le Vaillant, F.; Mateos Calbet, A.; Gonzalez-Pelayo, S.; Reijerse, E. J.; Ni, S.; Busch, J.; Cornella, J. Catalytic Synthesis of Phenols with Nitrous Oxide. *Nature* 2022, 604, 677–683.

(7) Taira, J.; Umei, T.; Inoue, K.; Kitamura, M.; Berenger, F.; Sacchettini, J. C.; Sakamoto, H.; Aoki, S. Improvement of the Novel Inhibitor for Mycobacterium Enoyl-Acyl Carrier Protein Reductase (InhA): A Structure–Activity Relationship Study of KES4 Assisted by in Silico Structure-Based Drug Screening. *J. Antibiot.* 2020, 73, 372–381.

(8) Zhang, X.; Thummuri, D.; Liu, X.; Hu, W.; Zhang, P.; Khan, S.; Yuan, Y.; Zhou, D.; Zheng, G. Discovery of PROTAC BCL-XL Degraders as Potent Anticancer Agents with Low on-Target Platelet Toxicity. *Eur. J. Med. Chem.* 2020, 192, 112186–112186.

(9) Li, H.; Gao, M. Q.; Chen, Y.; Wang, Y. X.; Zhu, X. L.; Yang, G. F. Discovery of Pyrazine-Carboxamide-Diphenyl-Ethers as Novel Succinate Dehydrogenase Inhibitors via Fragment Recombination. *J. Agric. Food Chem.* 2020, 68, 14001–14008.

(10) Olah, G. A. *Friedel–Crafts Chemistry*; Wiley-VCH: 1973.

(11) Huang, C.; Chattopadhyay, B.; Gevorgyan, V. Silanol: A Traceless Directing Group for Pd-Catalyzed *o*-Alkenylation of Phenols. *J. Am. Chem. Soc.* 2011, 133, 12406–12409.

(12) Dai, H.-X.; Li, G.; Zhang, X.-G.; Stepan, A. F.; Yu, J.-Q. Pd(II)-Catalyzed *ortho*- or *meta*-C–H Olefination of Phenol Derivatives. *J. Am. Chem. Soc.* 2013, 135, 7567–7571.

(13) John, A.; Nicholas, K. M. Palladium Catalyzed C–H Functionalization of O-Arylcarbamates: Selective *ortho*-Bromination using NBS. *J. Org. Chem.* 2012, 77, 5600–5605.

(14) Gong, T. J.; Xiao, B.; Liu, Z. J.; Wan, J.; Xu, J.; Luo, D. F.; Fu, Y.; Liu, L. Rhodium-Catalyzed Selective C–H Activation/Olefination of Phenol Carbamates. *Org. Lett.* 2011, 13, 3235–3237.

(15) Saphier, M. A Process for Substitution on Aromatic Rings. WO2010061382A2, 2010.

(16) Mitchell, S. C.; Waring, R. H. Aminophenols. *Ullmann's Encyclopedia of Industrial Chemistry* 2012, 59–78.

(17) Firouzabadi, H.; Iranpoor, N.; Zolfogol, M. A. Dinitrogen Tetroxide Complexes of Iron and Coppernitrates as New Reagents for Selective Mono- and Dinitration of Phenolic Compounds. *Synth. Commun.* 1997, 27, 3301–3311.

(18) Chen, K.; Kang, Q.-K.; Li, Y.; Wu, W.-Q.; Zhu, H.; Shi, H. Catalytic Amination of Phenols with Amines. *J. Am. Chem. Soc.* 2022, 144, 1144–1151.

(19) Rengshausen, S.; Etscheidt, F.; Großkurth, J.; Luska, K. L.; Bordet, A.; Leitner, W. Catalytic Hydrogenolysis of Substituted Diaryl Ethers by Using Ruthenium Nanoparticles on an Acidic Supported Ionic Liquid Phase (Ru@SILP-SO<sub>3</sub>H). *Synlett* 2019, 30, 405–412.

(20) Wang, M.; Liu, M.; Li, H.; Zhao, Z.; Zhang, X.; Wang, F. Dealkylation of Lignin to Phenol via Oxidation–Hydrogenation Strategy. *ACS Catal.* 2018, 8, 6837–6843.

(21) Van den Bosch, S.; Schutyser, W.; Vanholme, R.; Driessens, T.; Koelewijn, S.-F.; Renders, T.; De Meester, B.; Huijgen, W. J. J.; Dehaen, W.; Courtin, C. M.; Lagrain, B.; Boerjan, W.; Sels, B. F. Reductive Lignocellulose Fractionation into Soluble Lignin-Derived Phenolic Monomers and Dimers and Processable Carbohydrate Pulps. *Energy Environ. Sci.* 2015, 8, 1748–1763.

(22) Gao, F.; Webb, J. D.; Hartwig, J. F. Chemo- and Regioselective Hydrogenolysis of Diaryl Ether C–O Bonds by a Robust Heterogeneous Ni/C Catalyst: Applications to the Cleavage of Complex Lignin-Related Fragments. *Angew. Chem., Int. Ed.* 2016, 55, 1474–1478.

(23) Nichols, J. M.; Bishop, L. M.; Bergman, R. G.; Ellman, J. A. Catalytic C–O Bond Cleavage of 2-Aryloxy-1-Arylethanols and its Application to the Depolymerization of Lignin-Related Polymers. *J. Am. Chem. Soc.* 2010, 132, 16725–16725.

(24) Kusumoto, S.; Nozaki, K. Direct and Selective Hydrogenolysis of Arenols and Aryl Methyl Ethers. *Nat. Commun.* 2015, 6, 1–7.

(25) Arakawa, Y.; Minagawa, K.; Imada, Y. Advanced Flavin Catalysts Elaborated with Polymers. *Polym. J.* 2018, 50, 941–949.

(26) Takahashi, T.; Yoshimura, M.; Suzuka, H.; Maegawa, T.; Sawama, Y.; Monguchi, Y.; Sajiki, H. Chemoselective Hydrogenation using Molecular Sieves-Supported Pd Catalysts: Pd/MSA and Pd/MSSA. *Tetrahedron* 2012, 68, 8293–8299.

- (27) Song, S.; Yin, W.; Sun, X.; Cui, B.; Huang, L.; Li, P.; Yang, L.; Zhou, J.; Deng, Y. Anthranilic Acid from Ralstonia Solanacearum Plays Dual Roles in Intraspecies Signalling and Inter-Kingdom Communication. *ISME Journal* **2020**, *14*, 2248–2260.
- (28) Rahimi, A.; Ulbrich, A.; Coon, J. J.; Stahl, S. S. Formic-Acid-Induced Depolymerization of Oxidized Lignin to Aromatics. *Nature* **2014**, *S15*, 249–252.
- (29) Barker, J. L.; Frost, J. W. Microbial Synthesis of *p*-Hydroxybenzoic Acid from Glucose. *Biotechnol. Bioeng.* **2001**, *76*, 376–390.
- (30) Kitade, Y.; Hashimoto, R.; Suda, M.; Hiraga, K.; Inui, M. Production of 4-Hydroxybenzoic Acid by an Aerobic Growth-Arrested Bioprocess Using Metabolically Engineered *Corynebacterium glutamicum*. *Appl. Environ. Microbiol.* **2018**, *84*, 1–12.
- (31) Givens, R. S.; Stensrud, K.; Conrad, P. G.; Yousef, A. L.; Perera, C.; Senadheera, S. N.; Heger, D.; Wirz, J. *p*-Hydroxyphenacyl Photoremovable Protecting Groups Robust Photochemistry Despite Substituent Diversity. *Can. J. Chem.* **2011**, *89*, 364–384.
- (32) Béreau, V.; Jubéra, V.; Arnaud, P.; Kaiba, A.; Guionneau, P.; Sutter, J. P. Modulation of the Luminescence Quantum Efficiency for Blue Luminophor ( $\text{Al}(\text{salophen})^+$ ) by Ester-Substituents. *J. Chem. Soc., Dalton Trans.* **2010**, *39*, 2070–2077.
- (33) Hosseini-Sarvari, M.; Tavakolian, M.  $\text{Al}_2\text{O}_3/\text{MeSO}_3\text{H}$  (AMA) as a Novel Heterogeneous System for the Nitration of Aromatic Compounds by Magnesium Nitrate Hexahydrate. *J. Chem. Res.* **2008**, *2008*, 722–724.
- (34) Xue, L.; Su, W.; Lin, Z. Mechanism of Silver- and Copper-Catalyzed Decarboxylation Reactions of Aryl Carboxylic Acids. *Dalton Trans.* **2011**, *40*, 11926–11936.
- (35) Grainger, R.; Cornell, J.; Blakemore, D. C.; Larrosa, I.; Campanera, J. M. The *ortho*-Substituent Effect on the Ag-Catalysed Decarboxylation of Benzoic Acids. *Chem. Eur. J.* **2014**, *20*, 16680–16687.
- (36) Shang, R. *New Carbon–Carbon Coupling Reactions Based on Decarboxylation and Iron-Catalyzed C–H Activation*; University of Science and Technology of China: 2017.
- (37) Gooßen, L. J.; Thiel, W. R.; Rodríguez, N.; Linder, C.; Melzer, B. Copper-Catalyzed Protodecarboxylation of Aromatic Carboxylic Acids. *Adv. Synth. Catal.* **2007**, *349*, 2241–2246.
- (38) Seo, S.; Taylor, J. B.; Greaney, M. F. Protodecarboxylation of Benzoic Acids Under Radical Conditions. *Chem. Commun.* **2012**, *48*, 8270–8272.
- (39) Gooßen, L. J.; Linder, C.; Rodríguez, N.; Lange, P. P.; Fromm, A. Silver-Catalysed Protodecarboxylation of Carboxylic Acids. *Chem. Commun.* **2009**, *46*, 7173–7175.
- (40) Dupuy, S.; Lazreg, F.; Slawin, A. M. Z.; Cazin, C. S. J.; Nolan, S. P. Decarboxylation of Aromatic Carboxylic Acids by Gold(I)-N-Heterocyclic Carbene (NHC) Complexes. *Chem. Commun.* **2011**, *47*, 5455–5457.
- (41) Dickstein, J. S.; Mulrooney, C. A.; O'Brien, E. M.; Morgan, B. J.; Kozlowski, M. C. Development of a Catalytic Aromatic Decarboxylation Reaction. *Org. Lett.* **2007**, *9*, 2441–2444.
- (42) Sun, Z. M.; Zhang, J.; Zhao, P. Rh(I)-Catalyzed Decarboxylative Transformations of Arenecarboxylic acids: Ligand- and Reagent-Controlled Selectivity Toward Hydrodecarboxylation or Heck-mizoroki Products. *Org. Lett.* **2010**, *12*, 992–995.
- (43) Cohen, L. A.; Jones, W. M. A Study of pH Dependence in the Decarboxylation of *p*-Hydroxycinnamic Acid. *J. Am. Chem. Soc.* **1960**, *82*, 1907–1911.
- (44) Nomura, E.; Hosoda, A.; Mori, H.; Tanguchi, H. Rapid Base-Catalyzed Decarboxylation and Amide-Forming Reaction of Substituted Cinnamic Acids via Microwave Heating. *Green Chem.* **2005**, *7*, 863–866.
- (45) Langanke, J.; Slutz, E.; Heijl, J.; Meine, N. Verfahren Zur Herstellung Einer Hydroxyverbindung Durch Decarboxylierung In Anwesenheit Einer Brönsted-Base. WO2020114927A1, 2020.
- (46) Meine, N.; Slutz, E.; Heijl, J. Verfahren zur Herstellung einer Hydroxyverbindung durch Decarboxylierung. EP3663277A1, 2018.
- (47) Sharma, A.; Kumar, R.; Sharma, N.; Kumar, V.; Sinha, A. K. Unique Versatility of Ionic Liquids as Clean Decarboxylation Catalyst Cum Solvent: A Metal- and Quinoline-Free Paradigm Towards Synthesis of Indoles, Styrenes, Stilbenes and Arene Derivatives Under Microwave Irradiation in Aqueous Conditions. *Adv. Synth. Catal.* **2008**, *350*, 2910–2920.
- (48) Liu, D.; Sun, J.; Simmons, B. A.; Singh, S. N-Heterocyclic Carbene Promoted Decarboxylation of Lignin-Derived Aromatic Acids. *ACS Sus. Chem. Eng.* **2018**, *6*, 7232–7238.
- (49) Bordet, A.; Leitner, W. Metal Nanoparticles Immobilized on Molecularly Modified Surfaces: Versatile Catalytic Systems for Controlled Hydrogenation and Hydrogenolysis. *Acc. Chem. Res.* **2021**, *S4*, 2144–2157.
- (50) Luska, K. L.; Bordet, A.; Tricard, S.; Sinev, I.; Grünert, W.; Chaudret, B.; Leitner, W. Enhancing the Catalytic Properties of Ruthenium Nanoparticle-SILP Catalysts by Dilution with Iron. *ACS Catal.* **2016**, *6*, 3719–3726.
- (51) El Sayed, S.; Bordet, A.; Weidenthaler, C.; Hetaba, W.; Luska, K. L.; Leitner, W. Selective Hydrogenation of Benzofurans Using Ruthenium Nanoparticles in Lewis Acid-Modified Ruthenium-Supported Ionic Liquid Phases. *ACS Catal.* **2020**, *10*, 2124–2130.
- (52) Bordet, A.; Moos, G.; Welsh, C.; Licence, P.; Luska, K. L.; Leitner, W. Molecular Control of the Catalytic Properties of Rhodium Nanoparticles in Supported Ionic Liquid Phase (SILP) Systems. *ACS Catal.* **2020**, *10*, 13904–13912.
- (53) Renghausen, S.; Van Stappen, C.; Levin, N.; Tricard, S.; Luska, K. L.; DeBeer, S.; Chaudret, B.; Bordet, A.; Leitner, W. Organometallic Synthesis of Bimetallic Cobalt-Rhodium Nanoparticles in Supported Ionic Liquid Phases ( $\text{Co}_x\text{Rh}_{100-x}$ @SILP) as Catalysts for the Selective Hydrogenation of Multifunctional Aromatic Substrates. *Small* **2021**, *17*, 2006683–2006683.
- (54) Bordet, A.; El Sayed, S.; Sanger, M.; Boniface, K. J.; Kalsi, D.; Luska, K. L.; Jessop, P. G.; Leitner, W. Selectivity Control in Hydrogenation Through Adaptive Catalysis using Ruthenium Nanoparticles on a  $\text{CO}_2$ -Responsive Support. *Nat. Chem.* **2021**, *13*, 916–922.
- (55) Luza, L.; Rambor, C. P.; Gual, A.; Alves, F. J.; Eberhardt, D.; Dupont, J. Revealing Hydrogenation Reaction Pathways on Naked Gold Nanoparticles. *ACS Catal.* **2017**, *7*, 2791–2799.
- (56) Qadir, M. I.; Weilhard, A.; Fernandes, J. A.; de Pedro, I.; Vieira, B. J. C.; Waerenborgh, J. C.; Dupont, J. Selective Carbon Dioxide Hydrogenation Driven by Ferromagnetic RuFe Nanoparticles in Ionic Liquids. *ACS Catal.* **2018**, *8*, 1621–1627.
- (57) Sisodiya-Amrute, S.; Van Stappen, C.; Renghausen, S.; Han, C.; Sodreau, A.; Weidenthaler, C.; Tricard, S.; DeBeer, S.; Chaudret, B.; Bordet, A.; Leitner, W. Bimetallic  $\text{M}_x\text{Ru}_{100-x}$  Nanoparticles ( $\text{M} = \text{Fe}, \text{Co}$ ) on Supported Ionic Liquid Phases ( $\text{M}_x\text{Ru}_{100-x}$ @SILP) as Hydrogenation Catalysts: Influence of M and M:Ru Ratio on Activity and Selectivity. *J. Catal.* **2022**, *407*, 141–148.
- (58) Offner-Marko, L.; Bordet, A.; Moos, G.; Tricard, S.; Renghausen, S.; Chaudret, B.; Luska, K. L.; Leitner, W. Bimetallic Nanoparticles in Supported Ionic Liquid Phases as Multifunctional Catalysts for the Selective Hydrodeoxygénéation of Aromatic Substrates. *Angew. Chem., Int. Ed.* **2018**, *57*, 12721–12726.
- (59) Goclik, L.; Offner-Marko, L.; Bordet, A.; Leitner, W. Selective Hydrodeoxygénéation of Hydroxyacetophenones to Ethyl-Substituted Phenol Derivatives using a  $\text{FeRu}$ @SILP Catalyst. *Chem. Commun.* **2020**, *56*, 9509–9512.
- (60) Goclik, L.; Walschus, H.; Bordet, A.; Leitner, W. Selective Hydrodeoxygénéation of Acetophenone Derivatives using a  $\text{Fe}_{25}\text{Ru}_{75}$ @SILP Catalyst: A Practical Approach to the Synthesis of Alkyl Phenols and Anilines. *Green Chem.* **2022**, *24*, 2937–2945.
- (61) Dierks, M.; Cao, Z.; Manayil, J. C.; Akilavasan, J.; Wilson, K.; Schüth, F.; Rinaldi, R. Impact of Hydrophobic Organohybrid Silicas on the Stability of  $\text{Ni}_2\text{P}$  Catalyst Phase in the Hydrodeoxygénéation of Biophenols. *ChemCatChem.* **2018**, *10*, 2219–2231.
- (62) Insyani, R.; Verma, D.; Kim, S. M.; Kim, J. Direct One-Pot Conversion of Monosaccharides into High-Yield 2,5-Oimethylfuran over a Multifunctional Pd/Zr-based Metal-Organic Framework@

Sulfonated Graphene Oxide Catalyst. *Green Chem.* **2017**, *19*, 2482–2490.

(63) Scheuermeyer, M.; Kusche, M.; Agel, F.; Schreiber, P.; Maier, F.; Steinrück, H. P.; Davis, J. H.; Heym, F.; Jess, A.; Wasserscheid, P. Thermally Stable bis(trifluoromethylsulfonyl)imide Salts and their Mixtures. *New J. Chem.* **2016**, *40*, 7157–7161.

(64) Zhao, W.; Sun, J. Triflimide ( $\text{HNTf}_2$ ) in Organic Synthesis. *Chem. Rev.* **2018**, *118*, 10349–10392.

(65) Dilasari, B.; Jung, Y.; Kim, G.; Kwon, K. Effect of Cation Structure on Electrochemical Behavior of Lithium in  $[\text{NTf}_2]$ -based Ionic Liquids. *ACS Sus. Chem. Eng.* **2016**, *4*, 491–496.

(66) Rennie, A. J. R.; Martins, V. L.; Torresi, R. M.; Hall, P. J. Ionic Liquids Containing Sulfonium Cations as Electrolytes for Electrochemical Double Layer Capacitors. *J. Chem. Phys. C* **2015**, *119*, 23865–23874.

(67) Anslyn, E. V.; Dougherty, D. A. *Modern Physical Organic Chemistry*; University Science Books: 2006.

(68) Deng, F.; Huang, J.; Ember, E. E.; Achterhold, K.; Dierolf, M.; Jentys, A.; Liu, Y.; Pfeiffer, F.; Lercher, J. A. On the Mechanism of Catalytic Decarboxylation of Carboxylic Acids on Carbon-Supported Palladium Hydride. *ACS Catal.* **2021**, *11*, 14625–14634.

(69) Dunn, G. E.; Dayal, S. K. Mechanism of Decarboxylation of Substituted Anthranilic Acids at High Acidity. *Can. J. Chem.* **1970**, *48*, 3349–3353.

(70) Lin, J.; Wang, P.; Zhang, Z.; Xue, G.; Zha, D.; Wang, J.; Xu, X.; Li, Z. Facile Synthesis and Anti-Proliferative Activity Evaluation of Quinoxaline Derivatives. *Synth. Commun.* **2020**, *50*, 823–830.